crystals

MDPI

Article

Extended π-Systems in Diimine Ligands in [Cu(P^P)(N^N)][PF$_6$] Complexes: From 2,2'-Bipyridine to 2-(Pyridin-2-yl)Quinoline

Sarah Keller, Murat Alkan-Zambada, Alessandro Prescimone, Edwin C. Constable and Catherine E. Housecroft *

Department of Chemistry, University of Basel, BPR 1096, Mattenstrasse 24a, CH-4058 Basel, Switzerland; sarah.keller@chimieparistech.psl.eu (S.K.); murat.alkan@epfl.ch (M.A-Z.); alessandro.prescimone@unibas.ch (A.P.); edwin.constable@unibas.ch (E.C.C.)

* Correspondence: catherine.housecroft@unibas.ch; Tel: +41 61 207 1008

Received: 9 March 2020; Accepted: 26 March 2020; Published: 27 March 2020

Abstract: We describe the synthesis and characterization of [Cu(POP)(**1**)][PF$_6$], [Cu(POP)(**2**)][PF$_6$], [Cu(xantphos)(**1**)][PF$_6$], and [Cu(xantphos)(**2**)][PF$_6$] in which ligands **1** and **2** are 2-(pyridin-2-yl)quinoline and 2-(6-methylpyridin-2-yl)quinoline, respectively. With 2,2'-bipyridine (bpy) as a benchmark, we assess the impact of the extended π-system on structural and solid-state photophysical properties. The single crystal structures of [Cu(POP)(**2**)][PF$_6$], [Cu(xantphos)(**1**)][PF$_6$], and [Cu(xantphos)(**2**)][PF$_6$] were determined and confirmed a distorted tetrahedral copper(I) coordination environment in each [Cu(P^P)(N^N)]$^+$ cation. The xanthene unit in [Cu(xantphos)(**1**)][PF$_6$] and [Cu(xantphos)(**2**)][PF$_6$] hosts the quinoline unit of **1**, and the 6-methylpyridine group of **2**. ^{1}H NMR spectroscopic data indicate that these different ligand orientations are also observed in acetone solution. In their crystal structures, the [Cu(POP)(**2**)]$^+$, [Cu(xantphos)(**1**)]$^+$, and [Cu(xantphos)(**2**)]$^+$ cations exhibit different edge-to-face and face-to-face π-interactions, but in all cases, the copper(I) centre is effectively protected by a ligand sheath. In [Cu(POP)(**2**)][PF$_6$], pairs of cations engage in an efficient face-to-face π-stacking embrace, and we suggest that this may contribute to this compound having the highest photoluminescence quantum yield (PLQY = 21%) of the series. With reference to data from the Cambridge Structural Database, we compare packing effects and PLQY data for the complexes incorporating 2-(pyridin-2-yl)quinoline and 2-(6-methylpyridin-2-yl)quinoline, with those of the benchmark bpy-containing compounds. We also assess the effect that Cu···O distances in the {Cu(POP)} and {Cu(xantphos)} domains of [Cu(P^P)(N^N)][X] compounds have on solid-state PLQY values.

Keywords: single crystal structure; copper; 2-(pyridin-2-yl)quinoline; bis(phosphane); heteroleptic complex; photoluminescence; Cu···O distance analysis

1. Introduction

Heteroleptic [Cu(P^P)(N^N)]$^+$ coordination complexes in which P^P is a wide bite-angle bisphosphane [1] and N^N is a derivative of 2,2'-bipyridine (bpy) or 1,10-phenanthroline (phen) are gaining in popularity as the emissive component in the active layer in light-emitting electrochemical cells (LECs) [2,3]. McMillin and coworkers first recognized that copper(I) coordination compounds with PPh$_3$ or P^P ligands and phen or bpy possess low-lying metal-to-ligand charge transfer (MLCT) excited states [4,5]. More recently, it has been demonstrated that many [Cu(PP)(NN)]$^+$ complexes exhibit thermally activated delayed fluorescence (TADF) [6,7]. Fast intersystem crossing from the lowest-lying singlet excited state to the triplet excited state (which is at only slightly lower energy) occurs. The long lifetime of the excited triplet state and its relatively slow phosphorescence permits

thermal repopulation of the singlet excited state with concomitant fluorescence. Thus, harvesting of the emission from both the excited singlet and triplet states significantly increases the photoluminescent quantum yield (PLQY). From a synthetic standpoint, the design of suitable P^P and N^N ligands to optimize the emission properties of $[Cu(P^P)(N^N)]^+$ complexes remains challenging. Typically, P^P is bis(2-(diphenylphosphanyl)phenyl)ether (POP, IUPAC PIN oxydi(2,1-phenylene)]bis(diphenylphosphane)) or 4,5-bis(diphenylphosphanyl)-9,9-dimethyl-9*H*-xanthene (xantphos, IUPAC PIN (9,9-dimethyl-9*H*-xanthene-4,5-diyl)bis(diphenylphosphane)), both of which are commercially available.

Although the emissive behaviours of $[Cu(P^P)(N^N)]^+$ complexes containing a large variety of diimine ligands have been investigated, it is often the case that 'simpler is better' [8–11]. Some of the highest PLQY values and best-performing LECs have been observed for $[Cu(P^P)(N^N)]^+$ emitters in which N^N comprises 6-alkyl-2,2'-bipyridines and 6,6'-dialkyl-2,2'-bipyridines [8,9], 6-alkyloxy-2,2'-bipyridines and 6,6'-bis(alkyloxy)-2,2'-bipyridines [10,11], and 6-thioalkyl-2,2'-bipyridines [10]. One structural feature that appears to be important is π-stacking of ligands within the coordination sphere of the copper atom which hinders flattening of the structure in the excited state [12]. It has also been reported that short $Cu\cdots O_{xantphos}$ contacts are detrimental to emission [13,14]. However, as long as POP and xantphos (Scheme 1) remain popular choices for the wide bite-angle bisphosphanes, the close approach of the O to Cu atom in a $[Cu(P^P)(N^N)]^+$ complex is difficult to avoid.

Given the emissive behaviour of 6-alkyl-2,2'-bipyridines and the knowledge that π-stacking is beneficial, we decided to investigate the effects of extending the π-framework of the N^N domain by replacing the bpy scaffold by 2-(pyridin-2-yl)quinoline. Here, we report the preparation and characterization of $[Cu(P^P)(N^N)][PF_6]$ in which P^P is POP or xantphos and N^N is 2-(pyridin-2-yl)quinoline (**1**) or 2-(6-methylpyridin-2-yl)quinoline (**2**) (Scheme 1), and compare the properties and structures of these complexes with those of $[Cu(POP)(N^N)]^+$ and $[Cu(xantphos)(N^N)]^+$ in which N^N = bpy and 6-methyl-2,2'-bipyridine (6-Mebpy) [8,9,15–17].

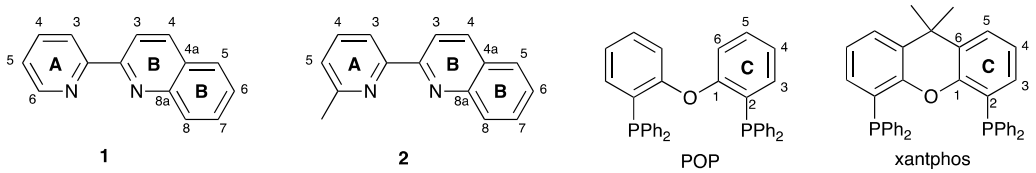

Scheme 1. Structures of the N^N and P^P ligands with atom labelling for the NMR assignments. In POP and xantphos, the phenyl rings are labelled **D**.

2. Materials and Methods

2.1. General

^1H, $^{13}C\{^1H\}$ and $^{31}P\{^1H\}$ NMR spectra were recorded at 298 K on a Bruker Avance III-500 NMR spectrometer (Bruker BioSpin AG, Fällanden, Switzerland), and ^1H and ^{13}C NMR chemical shifts were referenced to residual solvent peaks with respect to δ(TMS) = 0 ppm and ^{31}P NMR chemical shifts with respect to δ(85% aqueous H_3PO_4) = 0 ppm. Shimadzu LCMS-2020 (Shimadzu Schweiz GmbH, 4153 Reinach, Switzerland) and Bruker esquire 3000plus instruments (Bruker BioSpin AG, Fällanden, Switzerland) were used to record electrospray ionization (ESI) mass spectra with samples introduced. Solution absorption and emission spectra were recorded using Shimadzu UV-2600 spectrophotometer and Shimadzu RF-5301PC spectrofluorometer (Shimadzu Schweiz GmbH, 4153 Reinach, Switzerland), respectively.

Quantum yields were measured using a Hamamatsu absolute photoluminescence quantum yield spectrometer C11347 Quantaurus-QY. Emission lifetimes and powder emission spectra were measured with a Hamamatsu Compact Fluorescence lifetime Spectrometer C11367 Quantaurus-Tau, using an LED light source with λ_{exc} = 365 nm.

POP and xantphos were purchased from Acros Fisher Scientific AG, 4153 Reinach Switzerland) and Fluorochem (Chemie Brunschwig AG, 4052 Basel, Switzerland), respectively. $[Cu(MeCN)_4][PF_6]$

was prepared following the reported method [18]. 2-(Pyridin-2-yl)quinoline and (6-methylpyridin-2-yl)zinc(II) bromide were purchased from Sigma-Aldrich (Sigma Aldrich Chemie GmbH, 89555 Steinheim, Germany).

*2.2. 2-(6-Methylpyridin-2-yl)quinoline (**2**)*

We found the following procedure more convenient that the previously reported method [19]. Tetrakis(triphenylphosphine)palladium (58 mg, 0.05 mmol, 0.02 eq) and 2-chloroquinoline (411 mg, 2.51 mmol, 1.0 eq) were dissolved in dry THF (15 mL) and (6-methylpyridin-2-yl)zinc(II) bromide (9 mL, 0.5 M, 4.5 mmol, 1.8 eq.) was added. The mixture was stirred overnight at room temperature. The reaction was quenched by addition of aqueous $NaHCO_3$/H_4EDTA. The aqueous layer was washed with Et_2O (3 × 50 mL) and the combined organic layers dried over Na_2SO_4. The solvent was removed under reduced pressure and the crude product was purified by flash chromatography (CH_2Cl_2/*n*-pentane, 1:1, alumina) to obtain the product as a white solid (421 mg, 1.91 mmol). The ^1H NMR spectrum matched that reported [19,20] and also showed traces of residual 2-chloropyridine. The ligand was used without further purification.

*2.3. [Cu(POP)(**1**)][PF$_6$]*

POP (134 mg, 0.25 mmol, 1.0 eq) was added to a solution of [Cu(MeCN)$_4$][PF$_6$] (93 mg, 0.25 mmol, 1.0 eq) in CH_2Cl_2 (20 mL) and the colourless mixture was stirred for 2 h at room temperature. A solution of **1** (52 mg, 0.25 mmol, 1.0 eq) in CH_2Cl_2 (10 mL) was added, resulting in a yellow-orange solution which was stirred for another 2 h. The mixture was filtered, and the solvent was removed under reduced pressure. The crude product was redissolved in CH_2Cl_2 and layered with Et_2O to precipitate [Cu(POP)(**1**)][PF$_6$] (90 mg, 0.094 mmol, 38 %) as an orange microcrystalline solid. ^1H NMR (500 MHz, acetone-d_6) 8.92 (ddd, J = 5.2, 1.6, 0.8 Hz, 1H, H^{A6}), 8.77 (d, J = 8,7 Hz, 1H, H^{B4}), 8.68 (dt, J = 8.3, 1.0 Hz, 1H, H^{A3}), 8.63 (d, J = 8.7 Hz, 1H, H^{B3}), 8.34 (m, 1H, H^{B8}), 8.16 (m, 1H, H^{A4}), 8.05 (dd, J = 8.2, 1.4 Hz, 1H, H^{B5}), 7.58–7.53 (overlapping m, 2H, H^{A5+B6}), 7.46 (overlapping m, 2H, H^{C5}), 7.38 (t, J = 7.4 Hz, 2H, $H^{D4/D4'}$), 7.33-7.20 (overlapping m, 13H, $H^{C6+B7+D2/D2'+D3/D3'+D4/D4'}$), 7.14 (td, J = 7.5, 1.1 Hz, 2H, H^{C4}), 7.07 (t, J = 7.6 Hz, 4H, $H^{D3/D3'}$), 6.92 (m, 2H, H^{C3}), 6.87 (m, 4H, $H^{D2/D2'}$). $^{13}C\{^1H\}$ NMR (126 MHz, acetone-d_6): 159.2 (t, J = 6 Hz, C^{C1}), 153.3 ($C^{A2/B2}$), 153.1 ($C^{A2/B2}$), 150.9 (C^{A6}), 146.7 (C^{B4a}), 140.4 (C^{B4}), 139.8 (C^{A4}), 135.1 (C^{C3}), 134.3 (t, J = 8 Hz, $C^{D2/D2'}$), 133.4 (t, J = 8 Hz, $C^{D2/D2'}$), 133.3 (C^{C5}), 131.9 (t, J = 16 Hz, $C^{D1+D1'}$), 131.2 (C^{8a}), 130.7 ($C^{B7+D4/D4'}$), 130.4 ($C^{D4/D4'}$), 129.9 (C^{B8}), 129.8 (t, J = 5 Hz, $C^{D3/D3'}$), 129.5 (t, J = 5 Hz, $C^{D3/D3'}$), 129.3 (C^{B6}), 128.9 (C^{B5}), 127.4 (C^{A5}), 126.1 (t, J = 2 Hz, C^{C4}), 124.9 (t, J = 16 Hz, C^{C2}), 124.6 (C^{A3}), 121.3 (t, J = 2 Hz, C^{C6}), 119.9 (C^{B3}). $^{31}P\{^1H\}$ NMR (202 MHz, acetone-d_6): δ /ppm = −12.1 (br), −144.4 (sept, J_{PF} = 710 Hz). ESI-MS: m/z 807.1 $[M–PF_6]^+$ (base peak, calc. 807.2). Found C 62.76, H 4.25, N 3.16; $C_{50}H_{38}CuF_6N_2OP_3$ requires C 63.00, H 4.02, N 2.94%.

*2.4. [Cu(xantphos)(**1**)][PF$_6$]*

Compound **1** (52 mg, 0.25 mmol, 1.0 eq) and xantphos (145 mg, 0.25 mmol, 1.0 eq.) were dissolved in CH_2Cl_2 (20 mL) and the solution was stirred for 15 min. [Cu(MeCN)$_4$][PF$_6$] (93 mg, 0.25 mmol, 1.0 eq.) was dissolved in CH_2Cl_2 (20 mL) and stirred for 15 min after which the solution of xantphos and **1** was added. The reaction mixture turned yellow-orange and was stirred for 4.5 h. Then, it was filtered, and the solvent removed under reduced pressure. After recrystallization from CH_2Cl_2/Et_2O, [Cu(xantphos)(**1**)][PF$_6$] was obtained as a yellow-orange microcrystalline solid (242 mg, 0.244 mmol, 97%). ^1H NMR (500 MHz, acetone-d_6): δ/ppm: 8.92 (d, J = 5.1 Hz, 1H, H^{A6}), 8.83 (d, J = 8.7 Hz, 1H, H^{B4}), 8.76 (d, J = 8.1 Hz, 1H, H^{A3}), 8.71 (d, J = 8.7 Hz, 1H, H^{B3}), 8.22 (td, J = 7.9, 1.6 Hz, 1H, H^{A4}), 8.07 (d, J = 8.1 Hz, 1H, H^{B5}), 7.92 (dd, J = 7.8, 1.4 Hz, 1H, H^{C5}), 7.67 (m, 1H, H^{A5}), 7.52 (overlapping, 2H, H^{B6+B8}), 7.39 (m, 2H, $H^{D4'}$), 7.31–7.25 (overlapping m, 10H, $H^{D4+D2'+D3'}$), 7.23 (t, J = 7.8 Hz, 2H, H^{C4}), 7.08 (t, J = 7.6 Hz, 4H, H^{D3}), 6.89 (m, 1H, H^{B7}), 6.74 (m, 4H, H^{D2}), 6.55 (m, 2H, H^{C3}), 2.09 (s, 3H, $H^{Me\text{-}xantphos}$), 1.68 (s, 3H, $H^{Me\text{-}xantphos}$). $^{13}C\{^1H\}$ NMR (126 MHz, acetone-d_6): 156.2 (C^{C2}), 153.7 ($C^{A2/B2}$), 153.2 ($C^{A2/B2}$), 150.6 (C^{A6}), 146.9 (C^{B4a}), 140.5 (C^{B4}), 140.0 (C^{A4}), 135.0 (C^{C6}), 133.8 (t, J = 8 Hz, C^{D2}), 133.5 (t, J = 8 Hz, $C^{D2'}$), 132.7 (m, C^{D1}), 131.7 (C^{C3}), 131.4 (C^{B8a}), 131.2 (C^{B7}), 131.1 ($C^{D4/D4'}$), 131.0 ($C^{D4/D4'}$), 129.9 (t, J = 5 Hz,

$C^{D3'}$), 129.7 (t, J = 5 Hz, C^{D3}), 129.5 ($C^{B6/B8}$), 129.3 ($C^{B6/B8}$), 129.1 (C^{B5}), 128.6 (C^{C5}), 127.9 (C^{A5}), 126.4 (C^{C4}), 124.9 (C^{A3}), 121.5 (C^{C2}), 120.2 (C^{B3}), 37.6 ($C^{xantphos\ bridge}$), 30.9 ($C^{Me\text{-}xantphos}$), 25.6 ($C^{Me\text{-}xantphos}$). $^{31}P\{^{1}H\}$ NMR (202 MHz, acetone-d_6): δ/ppm = −12.3 (br), −144.4 (sept, J_{PF} = 707 Hz). ESI MS: m/z 847.1 $[M–PF_6]^+$ (base peak, calc. 847.2). Found: C 63.55, H 4.55, N 3.23 ($C_{53}H_{42}CuF_6N_2OP_3 \cdot 0.5H_2O$ requires C 63.51, H 4.32, N 2.79%).

*2.5. [Cu(POP)(**2**)][PF$_6$]*

A solution of POP (106 mg, 0.197 mmol, 1.0 eq) and **2** (52mg, 0.236 mmol, 1.2 eq.) in CH_2Cl_2 (20 mL) was added to a solution of $[Cu(MeCN)_4][PF_6]$ (73.4 mg, 0.197 mmol, 1.0 eq) in CH_2Cl_2 (20 mL) and the mixture was stirred for 3 h at room temperature. The mixture was filtered, and the solvent was removed under reduced pressure. The crude product was redissolved in CH_2Cl_2 and layered with Et_2O to yield [Cu(POP)(**2**)][PF_6] (158 mg, 0.163 mmol, 83%) as an orange microcrystalline solid. ^{1}H NMR (500 MHz, $(CD_3)_2CO$, 298 K): δ/ppm 8.66 (d, J = 8.7 Hz, 1H, H^{B4}), 8.42 (overlapping d, 2H, H^{A3+B3}), 8.29 (d, J = 8.9 Hz, 1H, H^{B8}), 8.10 (t, J = 7.8 Hz, 1H, H^{A4}), 8.04 (dd, J = 8.2, 1.2 Hz, 1H, H^{B5}), 7.57 (ddd, J = 8.4, 6.9, 1.1 Hz, 1H, H^{B6}), 7.54 (d, J = 7.6 Hz, 1H, H^{A5}), 7.51 (m, 2H, H^{C5}), 7.37–7.27 (overlapping m, 6H, $H^{C3+C4+D4/D4'}$), 7.25–7.14 (overlapping m, 9H, $H^{C6+B7+D4/D4'+D3/D3'}$), 7.08 (m, 4H, $H^{D2/D2'}$), 7.03–6.92 (m, 8H, $H^{D2/D2'+D3/D3'}$), 2.41 (s, 3H, H^{Me}). $^{13}C\{^{1}H\}$ NMR (126 MHz, acetone-d_6, 298 K): δ/ppm 160.1 (C^{A6}), 159.5 (t, J_{PC} = 6 Hz, C^{C1}), 154.1 ($C^{A2/B2}$), 152.9 ($C^{A2/B2}$), 146.4 (C^{B4a}), 140.2 (C^{B4}), 140.0 (C^{A4}), 134.8 (C^{C3}), 133.9 (t, J_{PC} = 8 Hz, $C^{D2/D2'}$), 133.6 (t, J_{PC} = 8 Hz, $C^{D2/D2'}$), 133.4 (C^{C5}), 132.6 (overlapping d, J_{PC} = 18 Hz, $C^{D1+D1'}$), 131.0 (C^{B7}), 130.9 ($C^{D4/D4'}$), 130.6 (overlapping $C^{D4/D4'+B8}$), 129.8 (C^{8a}), 129.6 (t, J_{PC} = 5 Hz, $C^{D3/D3'}$), 129.3 (t, J_{PC} = 5 Hz, $C^{D3/D3'}$), 129.1 (C^{B6}), 129.0 (C^{B5}), 127.7 (C^{A5}), 126.3 (t, J_{PC} = 2 Hz, C^{C4}), 125.9 (overlapping d, J_{PC} = 15 Hz, C^{C2}), 122.1 ($C^{A3/B3}$), 121.1 (t, J_{PC} = 2 Hz, C^{C6}), 120.1 ($C^{A3/B3}$), 27.2 (C^{Me}). $^{31}P\{^{1}H\}$ NMR (202 MHz, CD_2Cl_2): δ /ppm = −13.2 (br.), −144.4 (sept, J_{PF} = 710 Hz). ESI-MS: m/z 821.11 $[M–PF_6]^+$ (base peak, calc. 821.19), 601.00 $[M–\mathbf{2}–PF_6]^+$ (calc. 601.09). Found C 62.92, H 4.21, N 2.96; $C_{51}H_{40}CuF_6N_2OP_3$ requires C 63.32, H 4.17, N 2.90.

*2.6. [Cu(xantphos)(**2**)][PF$_6$]*

A solution of $[Cu(MeCN)_4][PF_6]$ (73 mg, 0.197 mmol, 1.0 eq) in CH_2Cl_2 (10 mL) was stirred for 5 min and was then added to a solution of xantphos (114 mg, 0.197 mmol, 1.0 eq) and **2** (52 mg, 0.236 mmol, 1.2 eq) in CH_2Cl_2 (20 mL) which had previously been stirred for 15 min. The mixture was stirred for 5.5 h at room temperature, after which time it was filtered. The solvent was removed from the filtrate under reduced pressure and the crude product was redissolved in CH_2Cl_2 and. The product was precipitated by layering with Et_2O and the solid was washed with *n*-hexane and after filtration, was redissolved in CH_2Cl_2. Layering with Et_2O yielded [Cu(xantphos)(**2**)][PF_6] (110 mg, 0.109 mmol, 55 %) as orange crystals. ^{1}H NMR (500 MHz, acetone-d_6, 298 K): δ/ppm 8.68 (d, J = 8.8 Hz, 1H, H^{B4}), 8.52 (overlapping d, 2H, H^{A3+B3}), 8.13 (t, J = 7.8 Hz, 1H, H^{A4}), 8.06–8.01 (overlapping m, 2H, H^{B5+B8}), 7.88 (dd, J = 7.8, 1.3 Hz, 2H, H^{C5}), 7.61 (m, 1H, H^{B6}), 7.49 (d, J = 7.7 Hz, 1H, H^{A5}), 7.40 (t, J = 7.4 Hz, 2H, $H^{D4'}$), 7.35 (t, J = 7.4 Hz, 2H, H^{D4}), 7.28 (t, J = 7.8 Hz, 2H, H^{C4}), 7.28–7.21 (overlapping m, 5H, $H^{B7+D3'}$), 7.18–7.12 (overlapping m, 8H, $H^{D2'+D3}$), 7.03 (m, 4H, H^{D2}), 6.82 (m, 2H, H^{C3}), 2.03 (s, 3H, H^{MeA}), 1.88 (s, 3H, $H^{Me\text{-}xantphos}$), 1.80 (s, 3H, $H^{Me\text{-}xantphos}$). $^{13}C\{^{1}H\}$ NMR (126 MHz, acetone-d_6, 298 K): δ/ppm = 159.9 (C^{A6}), 155.9 (t, J_{PC} = 6 Hz, C^{C1}), 154.0 ($C^{A2/B2}$), 152.7 ($C^{A2/B2}$), 146.2 (C^{B4a}), 140.3 ($C^{A4/B4}$), 140.2 ($C^{A4/B4}$), 135.0 (t, J_{PC} = 2 Hz, C^{C6}), 134.2 (t, J_{PC} = 8 Hz, C^{D2}), 133.7 (t, J_{PC} = 7 Hz, $C^{D2'}$), 132.4 (t, J_{PC} = 16 Hz, $C^{D1/D1'}$), 132.1 (t, J_{PC} = 16 Hz, $C^{D1/D1'}$), 131.2–131.1 (overlapping, $C^{B7+C3+D4}$), 130.8 ($C^{D4'}$), 130.6 ($C^{B5/B8}$), 129.8 (C^{B8a}), 129.7 (t, J_{PC} = 5 Hz, $C^{D3/D3'}$), 129.6 (t, J_{PC} = 5 Hz, $C^{D3/D3'}$), 129.5 (C^{B6}), 129.2 (C^{B6}), 129.1 ($C^{B5/B8}$), 128.6 (C^{C5}), 127.5 (C^{A5}), 126.5 (t, J_{PC} = 2 Hz, C^{C4}), 122.4 (C^{A3}), 122.2 (t, J_{PC} = 13 Hz, C^{C2}), 120.3 (C^{B3}), 37.2 ($C^{xantphos\text{-}bridge}$), 30.1 ($C^{Me\text{-}xantphos}$), 27.1 ($C^{Me\text{-}xantphos}$), 26.6 ($C^{MeA}$). $^{31}P\{^{1}H\}$ NMR (202 MHz, acetone-d_6): δ/ppm = −12.9 (br), −144.3 (sept, J_{PF} = 707 Hz). ESI MS: m/z 861.2 $[M–PF_6]^+$ (base peak, calc. 861.2). Found C 64.19, H 4.52, N 2.76; $C_{54}H_{44}CuF_6N_2OP_3$ requires C 64.38, H 4.40, N 2.78.

2.7. Crystallography

Single crystal data were collected on a Bruker APEX-II diffractometer (CuKα radiation) with data reduction, solution and refinement using the programs APEX [21] and CRYSTALS [22], or using a STOE StadiVari diffractometer equipped with a Pilatus300K detector and with a Metaljet D2 source (GaKα radiation) and solving the structure using Superflip [23,24] and Olex2 [25]. Structure analysis including the ORTEP representations, used Mercury CSD v. 4.1.1 [26,27].

*2.8. [Cu(xantphos)(**1**)][PF$_6$]*

$C_{53}H_{42}CuF_6N_2OP_3$, M_r = 993.38, yellow block, triclinic, space group *P*–1, *a* = 10.9132(6), *b* = 14.9862(9), *c* = 15.3881(9) Å, α = 83.394(3), β = 73.300(3), γ = 72.099(3)°, *V* = 2292.9(2) Å^3, D_c = 1.439 g cm^{-3}, *T* = 123 K, *Z* = 2, μ(CuKα) = 2.228 mm^{-1}. Total 26,926 reflections, 8415 unique (R_{int} = 0.034). Refinement of 7317 reflections (721 parameters) with $I > 2\sigma(I)$ converged at final R_1 = 0.0471 (R_1 all data = 0.0551), wR_2 = 0.1118 (wR_2 all data = 0.1182), gof = 0.9938. CCDC 1987595.

*2.9. [Cu(xantphos)(**2**)][PF$_6$]*

$C_{54}H_{44}CuF_6N_2OP_3$, M_r = 1007.41, yellow block, orthorhombic, space group *Pbca*, *a* = 19.3693(2), *b* = 20.3282(2), *c* = 23.2111(2) Å, *V* = 9139.21(15) Å^3, D_c = 1.464 g cm^{-3}, *T* = 130 K, *Z* = 8, μ(GaKα) = 3.604 mm^{-1}. Total 2,93,975 reflections, 9298 unique (R_{int} = 0.044). Refinement of 8499 reflections (604 parameters) with $I > 2\sigma(I)$ converged at final R_1 = 0.0563 (R_1 all data = 0.0607), wR_2 = 0.0500 (wR_2 all data = 0.0502), gof = 0.9997. CCDC 1987597.

*2.10. [Cu(POP)(**2**)][PF$_6$]*

$C_{54}H_{44}CuF_6N_2OP_3$, M_r = 1007.41, yellow block, triclinic, space group *P*–1, *a* = 11.7667(3), *b* = 12.4566(3), *c* = 16.3117(4) Å, α = 105.010(2), β = 93.514(2), γ = 108.465(2)°, *V* = 2163.43(10) Å^3, D_c = 1.485 g cm^{-3}, *T* = 130 K, *Z* = 2, μ(GaKα) = 3.790 mm^{-1}. Total 87292 reflections, 42829 unique (R_{int} = 0.058). Refinement of 7415 reflections (577 parameters) with $I > 2\sigma(I)$ converged at final R_1 = 0.0957 (R_1 all data = 0.1080), wR_2 = 0.0735 (wR_2 all data = 0.0738), gof = 0.8927. CCDC 1987596.

3. Results and Discussion

3.1. Characterization of Copper(I) Complexes

The base peak in the ESI mass spectrum of each [Cu(P^P)(N^N)][PF$_6$] compound corresponded to the [M–PF$_6$]$^+$ ion, and mass spectra are presented in Supplementary Figures S1–S4. In the $^{31}P\{^1H\}$ NMR spectrum of each complex, a broadened peak around δ −12 ppm (see Sections 2.3–2.6) was observed for the P^P ligand in addition to the septet for the [PF$_6$]$^-$ counterion. The ^1H and $^{13}C\{^1H\}$ NMR spectra were assigned using 2D methods and the HMQC and HMBC spectra are shown in Figures S5–S12 in the Supporting Information. Figure 1 displays a comparison of the ^1H NMR spectra of [Cu(POP)(**1**)][PF$_6$] and [Cu(POP)(**2**)][PF$_6$], and a similar comparison is made for the xantphos-containing compounds in Figure 2. In each complex, signals for H^{B3} and H^{B4} were distinguished using the NOESY cross-peak between H^{A3} and H^{B3}. The phenyl rings of the PPh_2 groups split into two sets, labelled D and D′. In the xantphos-containing compounds, the rigidity of the xanthene backbone leads to a ligand conformation in which two phenyl rings face towards the N^N ligand and two phenyls point away. A NOESY cross-peak between H^{A6} (on the N^N ligand) and H^{D2} (on xantphos) allows the D and D′ rings to be distinguished. In contrast, in the POP-containing complexes, the NOESY spectrum evidences conformational exchange (EXSY) peaks between pairs of signals for $H^{D2/D2'}$, $H^{D3/D3'}$, and $H^{D4/D4'}$ (Figure 3). This is readily rationalized in terms of the conformational flexibility of the POP ligand.

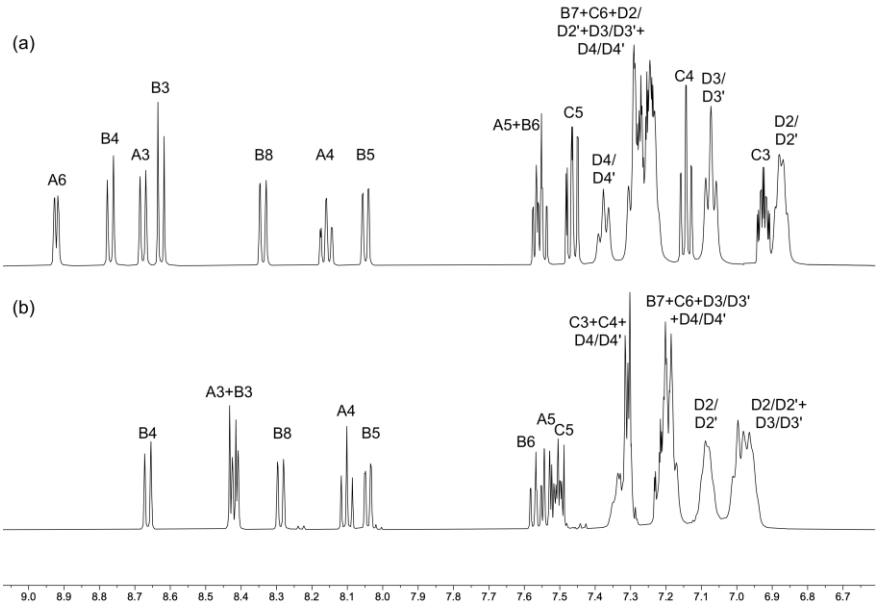

Figure 1. Comparison of the aromatic regions of the ^{1}H NMR spectra (500 MHz, acetone-d_6, 298 K) of (**a**) [Cu(POP)(**1**)][PF_6] and (**b**) [Cu(POP)(**2**)][PF_6]. See Scheme 1 for atom labelling. Scale: δ/ppm.

The major difference between Figures 1a and 1b is the disappearance of the resonance for proton H^{A6} corresponding to the introduction of the 6-methyl substituent in ligand **2**. In contrast, inspection of Figure 2 reveals that, in addition to the loss of the H^{A6} signal on going from [Cu(xantphos)(**1**)][PF_6] to [Cu(xantphos)(**2**)][PF_6], the signals for the quinoline protons H^{B7} and H^{B8} undergo significant movement to higher frequencies. The tetrahedral geometry of the copper atom (confirmed in the single crystal structures discussed later) leads to the mean planes through the P^P and N^N ligands being approximately orthogonal to one another. The N^N ligand can adopt one of two orientations with the quinoline unit pointing towards or away from the xanthene unit. As Figure 4 shows, this places protons H^{B7} and H^{B8} in very different environments. In the structural discussion that follows, we confirm that in the solid state, the N^N ligands in [Cu(xantphos)(**1**)]$^+$ and [Cu(xantphos)(**2**)]$^+$ adopt different orientations, and the ^{1}H NMR spectroscopic data are consistent with the retention of this difference in solution.

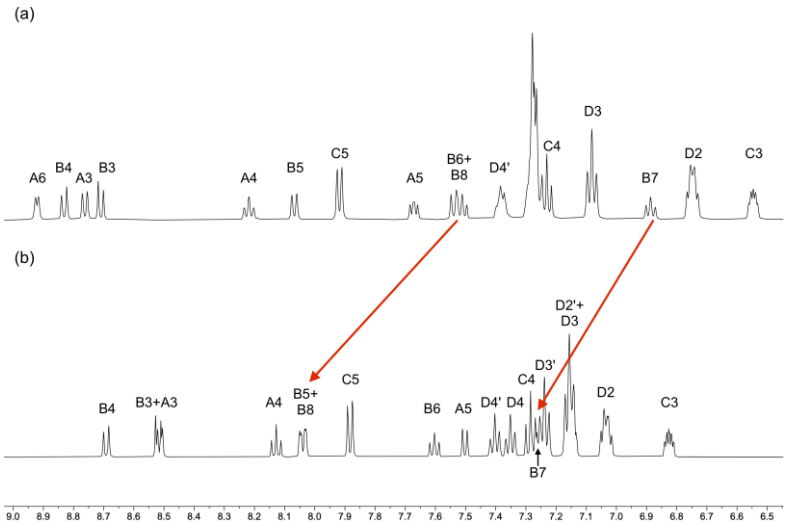

Figure 2. Comparison of the aromatic regions of the ^{1}H NMR spectra (500 MHz, acetone-d_6, 298 K) of (**a**) [Cu(xantphos)(**1**)][PF_6] and (**b**) [Cu(xantphos)(**2**)][PF_6]. See Scheme 1 for atom labelling. Scale: δ/ppm. Note the movement of the signals for quinoline protons H^{B7} and H^{B8} (see text).

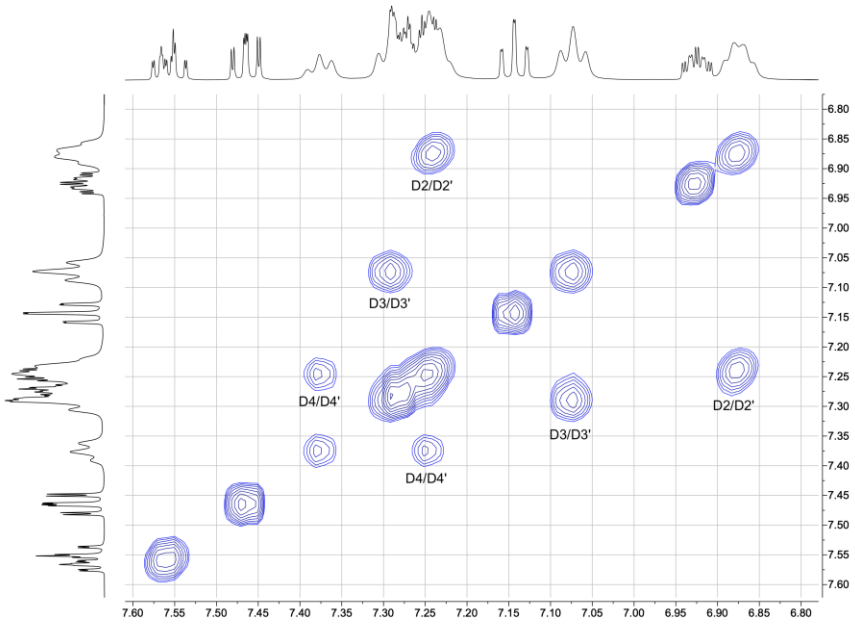

Figure 3. Part of the NOESY spectrum (500 Hz, 298 K, acetone-d_6) of [Cu(POP)(**1**)][PF_6] showing exchange (EXSY) cross-peaks.

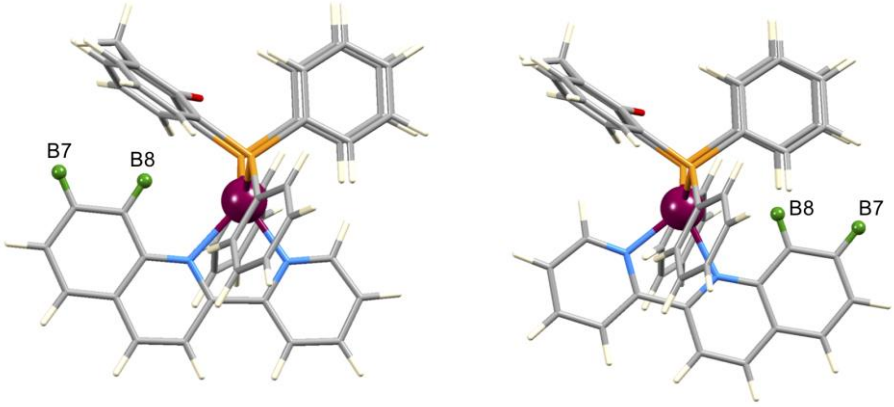

Figure 4. Modelled (Molecular Mechanics using Spartan '18 (v. 1.3) [28]) of two possible conformers of [Cu(xantphos)(**1**)]$^+$ illustrating the different environments of quinoline protons H^{B7} and H^{B8} in the two conformers.

3.2. Crystal Structures of [Cu(xantphos)(1)][PF6], [Cu(xantphos)(2)][PF6] and [Cu(POP)(2)][PF6]

Yellow single crystals of [Cu(xantphos)(**1**)][PF_6], [Cu(xantphos)(**2**)][PF_6] and [Cu(POP)(**2**)][PF_6] were grown from CH_2Cl_2 solutions layered with Et_2O. All compounds crystallize without lattice solvent, thereby allowing meaningful comparisons of the structures, including packing interactions. [Cu(xantphos)(**1**)][PF_6] and [Cu(POP)(**2**)][PF_6] crystallize in the triclinic space group *P*–1, while [Cu(xantphos)(**2**)][PF_6] crystallizes in the orthorhombic space group *Pbca*. ORTEP representations of the [Cu(P^P)(N^N)]$^+$ cations are shown in Figure 5 and selected bond lengths and angles are summarized in Table 1. Table 1 also includes values of Houser's τ_4 parameter which is used to quantify distortion at the copper centre along a path from T_d (τ_4 = 1.00) towards C_{3v} symmetry (τ_4 = 0.85) [29]. The τ_4 values in Table 1 indicate distorted C_{3v} symmetries, with larger distortions for [Cu(xantphos)(**2**)]$^+$ and [Cu(POP)(**2**)]$^+$ than for [Cu(xantphos)(**1**)]$^+$. In both [Cu(xantphos)(**2**)]$^+$, and [Cu(POP)(**2**)]$^+$, there is one large P–Cu–N bond angle (125.94(6)^o and 129.07(11)^o, Table 1) that contributes to the value of τ_4 = 0.79 and this is associated with a phenyl–2-(pyridin-2-yl)quinoline π-stacking contact (see later discussion).

Table 1. Bond lengths and angles in the coordination sphere of each [Cu(P^P)(N^N)]$^+$ cation.

Parameter	[Cu(xantphos)(1)]$^+$	[Cu(xantphos)(2)]$^+$	[Cu(POP)(2)]$^+$
Cu–N / Å	2.070(2), 2.083(2)	2.094(2), 2.096(2)	2.129(4), 2.043(4)
Cu–P / Å	2.2641(7), 2.2702(7)	2.2562(8), 2.3153(8)	2.3032(12), 2.2597(13)
P–Cu–P / °	112.24(3)	119.38(3)	117.59(5)
N–Cu–N / °	79.24(8)	79.05(9)	79.53(15)
P–Cu–N / °	118.13(6), 117.32(6), 115.99(6), 110.11(6)	122.31(6), 102.51(6), 125.94(6), 98.99(6)	129.07(11), 104.52(10), 119.73(11), 98.76(10)
τ_4 [1]	0.88	0.79	0.79

[1] τ_4 parameter, see reference [29].

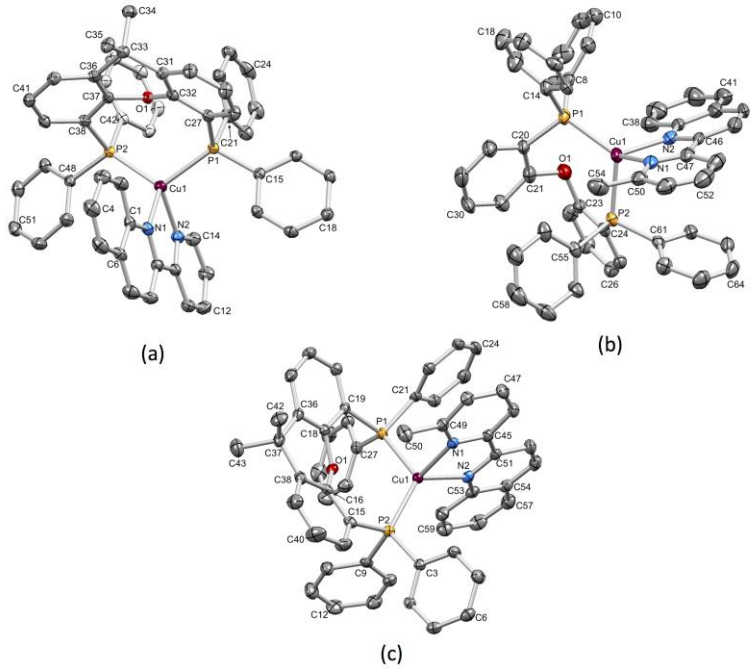

Figure 5. ORTEP representations of the structures of the complex cations in (**a**) [Cu(xantphos)(**1**)][PF$_6$], (**b**) [Cu(POP)(**2**)][PF$_6$], and (**c**) [Cu(xantphos)(**2**)][PF$_6$]. Ellipsoids are plotted at 40% probability level and H atoms are omitted for clarity.

A search of the Cambridge Structural Database (CSD) v. 5.41 [30] revealed that [Cu(xantphos)(**1**)][PF$_6$], [Cu(POP)(**2**)][PF$_6$], and [Cu(xantphos)(**2**)][PF$_6$] are the first examples of structurally characterized 2-(pyridin-2-yl)quinoline-containing [Cu(xantphos)(N^N)][PF$_6$] and [Cu(POP)(N^N)][PF$_6$] compounds. In each complex, the 2-(pyridin-2-yl)quinoline moiety is close to planar. The angles between the least squares planes of the pyridine and quinoline units are 6.5° in [Cu(xantphos)(**1**)]$^+$, 9.2° in [Cu(xantphos)(**2**)]$^+$, and 9.9° in [Cu(POP)(**2**)]$^+$. These values lie in the typical range for [Cu(POP)(N^N)]$^+$ and [Cu(xantphos)(N^N)]$^+$ complexes in which N^N is restricted to a bpy (excluding phen derivatives) or a 2,2′-biquinoline-based ligand (Figure 6). Interestingly, within this dataset, the deviation from planarity is quite severe in some cations, with the largest angle of 31.6° occurring in [Cu(xantphos)(N^N)][PF$_6$] in which N^N is 6,6'-dimethyl-4,4'-diphenyl-2,2'-bipyridine [31]. The biquinoline (biq) ligand may also undergo significant twisting, with angles of 15.5° in [Cu(xantphos)(biq)][PF$_6$] [32], 16.6° in [Cu(POP)(biq)][PF$_6$] [33] and 19.8° in [Cu(POP)(4,4′-Ph$_2$biq)][PF$_6$] [34]. Thus, the small twist angles in coordinated ligands **1** and **2** are not a consequence of the extended π-system on going from bpy to 2-(pyridin-2-yl)quinoline.

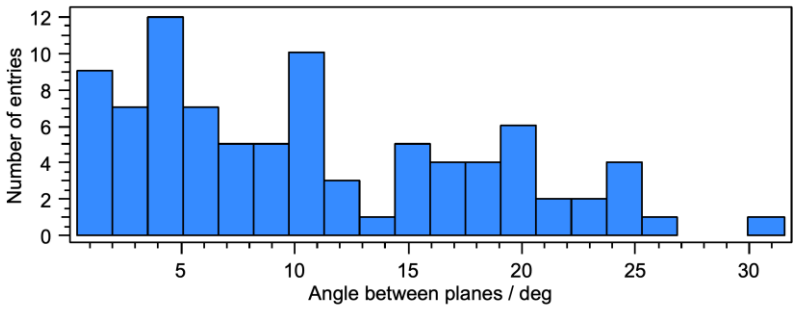

Figure 6. Distribution of angles between the planes of the pyridine rings in bpy or quinoline units in biquinoline ligands in [Cu(POP)(N^N)]$^+$ and [Cu(xantphos)(N^N)]$^+$ complexes. Data from the Cambridge Structural Database (CSD), version 5.41 [30], searched using Conquest version 2.0.4 [35].

As discussed in Section 3.1, there are two possible orientations of the N^N ligand in the xantphos-containing compounds. The xanthene unit possesses a 'bowl'-like conformation which, in many [Cu(P^P)(N^N)]$^+$ cations, hosts a substituent attached to the N^N ligand, see for example [9,10]. In [Cu(xantphos)(**1**)][PF_6] and [Cu(xantphos)(**2**)][PF_6], ligands **1** and **2** adopt different orientations as is shown in Figures 7a and 7b. Ligand **1** is oriented with the quinoline over the xanthene unit, in contrast to **2** which has the 6-methylpyridine group facing the xanthene 'bowl'. Figures 7c and 7d display space-filling representations of the complex cations, looking towards the xanthene unit. The arene ring of the quinoline (Figure 7c) and the methyl group of the 6-methylpyridine ring (Figure 7d) are neatly accommodated within the cavity of the xanthene unit. An additional difference between the structures concerns the intra-cation interactions between the phenyl rings (one from each PPh_2 group) and the N^N ligand. In [Cu(xantphos)(**1**)]$^+$, one *ortho*-H atom of each phenyl ring points towards the centre of the Cu(N^N) chelate ring with C–H···centroid distances of 2.67 Å and 2.89 Å (Figure 7a and 7c). In [Cu(xantphos)(**2**)]$^+$, ligand **2** is tilted so as to engage in a π-stacking interaction with one phenyl ring (Figure 7d); the angle between the planes of the rings containing C21 and N2 is 16.5° and the centroid···centroid distance is 3.90 Å. In [Cu(xantphos)(**1**)]$^+$, a face-to-face π-stacking contact is observed between the phenyl rings containing C21 and C42 (Figures 5a and 7a). The rings adopt a favourable offset arrangement, with a centroid···centroid separation of 3.84 Å and an inter-plane angle of 17.5°. In both [Cu(xantphos)(**1**)][PF_6] and [Cu(xantphos)(**2**)][PF_6], therefore, a combination of edge-to-face and face-to-face intra-cation contacts are observed and the copper centre is efficiently protected by the ligand sheath. We note that the Cu···O non-bonded distances are 3.199(2) Å in [Cu(xantphos)(**1**)]$^+$, and 3.075(2) Å in [Cu(xantphos)(**2**)]$^+$. For comparison, the Cu···O separation is 3.162(3) Å in [Cu(POP)(**2**)]$^+$. We return to the relevance of these distances in Section 3.4.

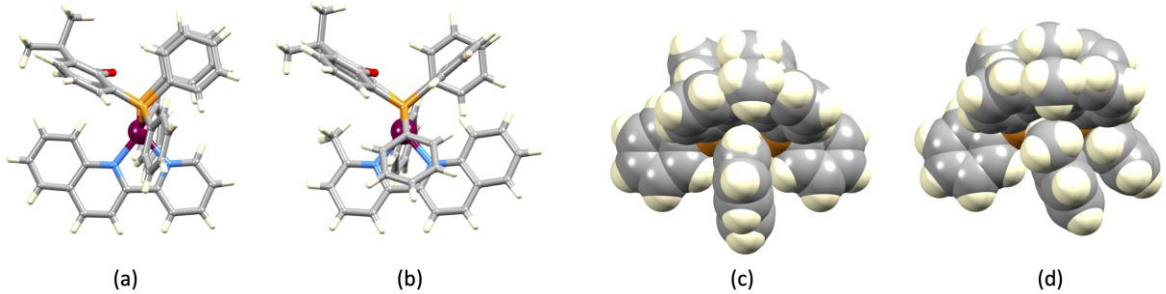

Figure 7. Views of the (**a**) [Cu(xantphos)(**1**)]$^+$ and (**b**) [Cu(xantphos)(**2**)]$^+$ cations illustrating the different orientations of **1** and **2** with respect to the xanthene unit. Spacefilling representations of (**c**) [Cu(xantphos)(**1**)]$^+$ and (**d**) [Cu(xantphos)(**2**)]$^+$ looking towards the xanthene 'bowl' (top of the figures).

The POP-containing complex exhibits only one π-stacking interaction for which the arrangement of the participating phenyl and pyridine rings (Figure 8a,b) is not optimal. The angle between the

ring planes is 20.4°, and the centroid···centroid distance is 4.03 Å. However, this weak contact is augmented by inter-cation packing interactions involving a centrosymmetric π-stacking embrace between the rings in ligands **2** containing N2 and N2i (symmetry code i = –*x*, 2–*y*, 1–*z*) (Figure 8c). The separation of the ring planes is 3.24 Å and the centroid···centroid distance is 3.73 Å. These parameters are consistent with an efficient interaction [36]. No analogous intermolecular interactions are observed in [Cu(xantphos)(**1**)][PF_6] and [Cu(xantphos)(**2**)][PF_6]. We note that in the solid state, [Cu(POP)(phen)][BF_4] also shows the assembly of centrosymmetric dimers through π-stacking of pairs of phen ligands [37].

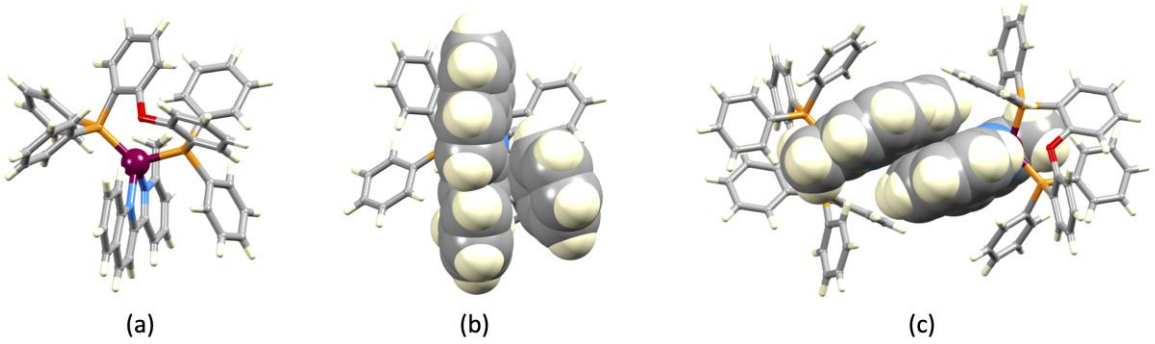

Figure 8. (**a**) and (**b**) Each [Cu(POP)(**2**)]$^+$ cation offers only one, non-optimal π-stacking interaction. (**c**) Pairs of cations engage in a centrosymmetric π-stacking embrace.

3.3. Photophysical Properties

Figure 9 illustrates the solution absorption spectra of the four copper(I) compounds and absorption maxima are given in Table 2. Bands below ca. 350 nm arise from ligand-centred π*←π transitions, and the broad absorption band at ca. 420–430 nm is assigned to MLCT. The latter shifts to higher energy (Table 2) on introducing the 6-methyl substituent into the pyridyl unit in keeping with observations for analogous compounds containing bpy and 6-Mebpy ligands [8,9,16]. The MLCT bands for all four compounds are red-shifted with respect to those for [Cu(POP)(bpy][PF_6] (388 nm) [16], [Cu(xantphos)(bpy][PF_6] (383 nm) [16], [Cu(POP)(6-Mebpy][PF_6] (380 nm) [8], and [Cu(xantphos)(6-Mebpy][PF_6] (379 nm) [9], consistent with the extended π-system in ligands **1** and **2**.

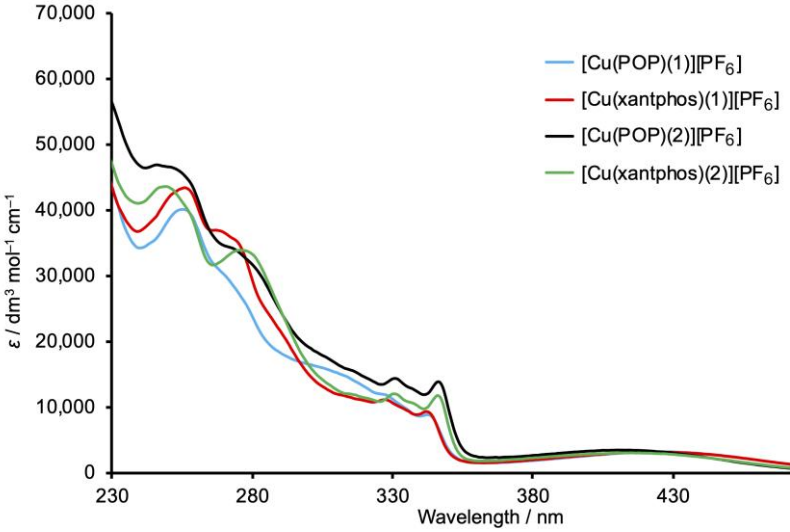

Figure 9. Solution absorption spectra of the copper(I) compounds in CH_2Cl_2 (2.5×10^{-5} mol dm^{-3} for complexes with ligand **1** and 2.1×10^{-5} mol dm^{-3} for those containing **2**.).

Table 2. Solution absorption maxima for the copper(I) compounds (CH_2Cl_2, 2.5×10^{-5} or 2.1×10^{-5} mol dm^{-3}).

Compound	λ_{max} / nm (ε / dm^3 mol^{-1} cm^{-1})	
	Ligand-Centred π*←π	MLCT
[Cu(POP)(**1**)][PF_6]	257 (39,800), 273 sh (28,600), 314 sh (15,800), 330 (11,200), 344 (8,500)	429 (3,200)
[Cu(xantphos)(**1**)][PF_6]	258 (42,800), 270 (36,500), 275 sh (35,000), 293 sh (19,600), 329 (10,950), 344 (8,800)	429 (3,200)
[Cu(POP)(**2**)][PF_6]	250 (46,500), 275 sh (33,600), 318 sh (15,000), 336 (12,950), 348 (13,000)	416 (3,400)
[Cu(xantphos)(**2**)][PF_6]	251 (43,200), 258 sh (39,300), 278 (33,700), 332 (11,800), 338 sh (10,400), 347 (11,500)	419 (2,900)

In CH_2Cl_2 solution, the compounds are weak emitters and we focus only on the solid-state properties. Emission data for powdered samples of the compounds are summarized in Table 3 and normalized emission spectra are depicted in Figure 10. The introduction of the 6-methyl group into the pyridine ring on going from **1** to **2** leads to a blue-shift in the emission maximum. Similar trends in values of λ^{em}_{max} are observed on going from [Cu(POP)(bpy)][PF_6] (581 nm) [16] to [Cu(POP)(6-Mebpy)][PF_6] (567 nm) [8], and from [Cu(xantphos)(bpy)][PF_6] (587 nm) [16] to [Cu(xantphos)(6-Mebpy)][PF_6] (547 nm) [9]. Introducing the methyl group to the N^N ligand leads to an enhancement of the PLQY (Table 3), and follows trends previously reported for bpy-based ligands [8,9]. A small enhancement in PLQY is observed when the bpy ligand in [Cu(POP)(bpy)][PF_6] and [Cu(POP)(bpy)][PF_6] is replaced by 2-(pyridin-2-yl)quinoline (**1**); compare PLQY values of 3.0% and 1.7% for powdered [Cu(POP)(bpy)][PF_6] and [Cu(xantphos)(bpy)][PF_6], respectively [16], with the data in Table 3. However, while a similar improvement is observed on going from [Cu(POP)(6-Mebpy)][PF_6] (PLQY = 9.5% [8]) to [Cu(POP)(**2**)][PF_6] (PLQY = 21%), the opposite is true for the xantphos-containing compounds. For [Cu(xantphos)(6-Mebpy)][PF_6], the PLQY = 34% [9] compared to 17% for [Cu(xantphos)(**2**)][PF_6]. The excited state lifetimes increase on going from ligand **1** to ligand **2** for both P^P ligands. This is consistent with less flattening of the coordination environment at the copper centre in the excited state upon introduction of the methyl group at the pyridyl ring. The excited state lifetime values are roughly doubled for the complexes with xantphos in comparison to those with POP. Lifetime decay plots are presented in Supplementary Figures S13–S24, including fitting curves (mono- and biexponential decay) and decay functions. The complexes were found to exhibit first-order decay of their excited state lifetimes.

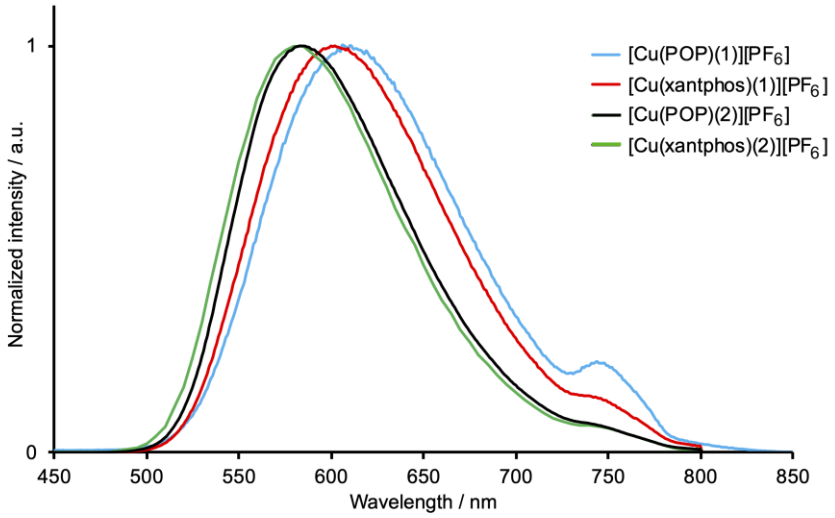

Figure 10. Normalized solid-state emission spectra of the compounds (λ_{exc} = 365 nm).

Table 3. Solid-state emission data (298 K) for the copper(I) compounds.

Compound	λ_{exc} / nm	λ^{em}_{max} / nm	PLQY / %	τ / μs
[Cu(POP)(**1**)][PF_6]	365	610	6	2.9
[Cu(xantphos)(**1**)][PF_6]	365	602	9	5.0
[Cu(POP)(**2**)][PF_6]	365	583	21	5.6
[Cu(xantphos)(**2**)][PF_6]	365	580	17	10.7

3.4. Comments on Structure–Property Relationships

One of the key challenges in improving the photoluminescence properties of $[Cu(P^P)(N^N)]^+$ species is the design of the N^N ligands, and selecting an appropriate combination of N^N and P^P ligands. In a light-emitting device such as a LEC, electroluminescence (EL), rather than photoluminescence (PL), becomes the critical phenomenon. Although it does not necessarily follow that high PLQY leads to high EL, it is usually true that low PL indicates a poor candidate for EL. In a LEC, the [Cu(P^P)(N^N)][X] emitters in the active layer are usually present in the form of thin films, for example, in an ionic liquid with a typical ratio of emitter:ionic liquid of 4:1. Thus, structural information obtained from single crystal structures becomes relevant for gaining insight into interactions both within the coordination sphere of the copper(I) centre and between the $[Cu(P^P)(N^N)]^+$ cations.

For the series of compounds investigated here, the highest solid-state PLQY was observed for [Cu(POP)(**2**)][PF_6]. Based on the work of Armaroli, Nierengarten, Delavaux-Nicot and coworkers [12], we asked whether π-stacking of ligands plays a role. While each of $[Cu(xantphos)(\mathbf{1})]^+$, $[Cu(POP)(\mathbf{2})]^+$, and $[Cu(xantphos)(\mathbf{2})]^+$ exhibits C–H···π and face-to-face intra-cation contacts, only $[Cu(POP)(\mathbf{2})]^+$ presents a supramolecularly assembled dimeric motif (Figure 8c). In the related compound [Cu(POP)(6-Mebpy)][PF_6], there is again a centrosymmetric dimeric motif in the solid-state involving the unsubstituted pyridine ring of 6-Mebpy (Figure 11a). This has not previously been described [8], and analysis of the packing (CSD refcode BOSVAI) reveals an inter-plane separation of 3.35 Å and a centroid···centroid distance of 3.74 Å. The tighter association of the cations in [Cu(POP)(**2**)][PF_6] (Figure 11b) may contribute to the enhanced PLQY of [Cu(POP)(**2**)][PF_6] (21%) compared to [Cu(POP)(6-Mebpy)][PF_6] (9.5% [8]). We note that $[Cu(POP)(bpy)]^+$ also assembles into dimeric motifs in the crystal structures of [Cu(POP)(bpy)][PF_6]·Et_2O (CSD refcode CAPZEZ) [17], and [Cu(POP)(bpy)][PF_6]·$CHCl_3$ (CSD refcode OYUKID) [15] as shown in Figure 11c. Analysis of the data from the CSD gives inter-plane and centroid···centroid distances of 3.62 Å and 3.86 Å, respectively, in [Cu(POP)(bpy)][PF_6]·Et_2O, and 3.45 Å and 3.97 Å, respectively, in [Cu(POP)(bpy)][PF_6]·$CHCl_3$. The similarities in the packing motifs in $[Cu(POP)(bpy)]^+$ (Figure 11c) and $[Cu(POP)(6\text{-Mebpy})]^+$ (Figure 11b, top) are striking, and it is interesting to note that the solid-state PLQY values are of the same orders of magnitude (3.0% and 9.5%, respectively [8,16]).

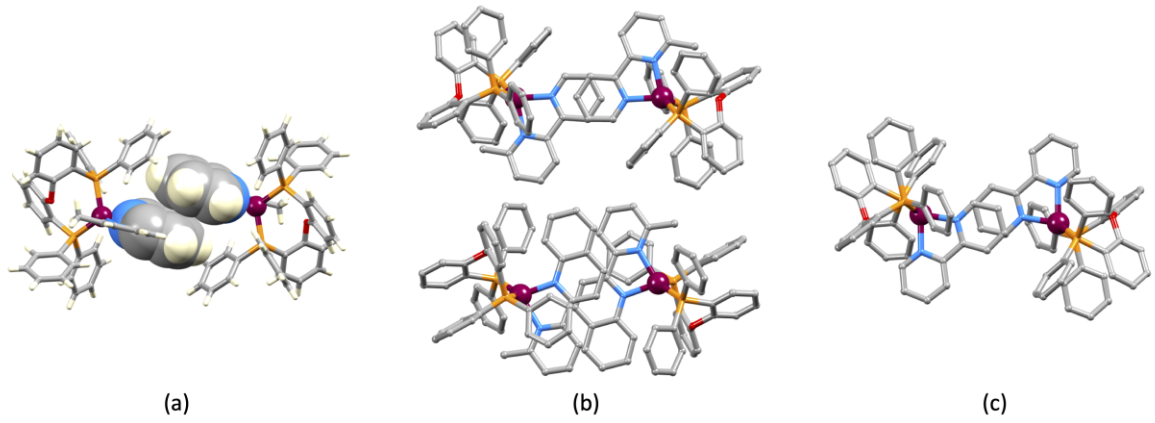

Figure 11. (**a**) Dimeric motif in the solid-state structure of [Cu(POP)(6-Mebpy)][PF_6] (CSD refcode BOSVAI), and (**b**) the same motif viewed from above, compared with the analogous packing unit in

[Cu(POP)(**2**)][PF_6] (H atoms omitted). (**c**) Centrosymmetric packing motif in the solid-state structure of [Cu(POP)(bpy)][PF_6]·Et_2O (CSD refcode CAPZEZ).

Finally, we return to the question of the effects of close Cu···O contacts in [Cu(POP)(N^N]$^+$ and [Cu(xantphos)(N^N]$^+$ complexes. The detailed investigations of Viciano-Chumillas, Costa and Cano focused on a series of xantphos-containing compounds [13,14]. We decided to attempt to correlate solid-state PLQY values of [Cu(POP)(N^N][X] and [Cu(xantphos)(N^N][X] complexes in which N^N is bpy or a derivative of bpy, and X^- is any anion, with the Cu···O distances in the cations. A search of the CSD [30] using Conquest, version 2.0.4 [35], was used to generate the results given in Table S1 in the supporting information. Only compounds for which solid-state PLQY data are available are included. Figure 12 presents a scatter plot of the data, with POP- and xantphos-containing compounds delineated by blue and orange markers, respectively. Data for [Cu(xantphos)(**1**)][PF_6], [Cu(POP)(**2**)][PF_6], and [Cu(xantphos)(**2**)][PF_6] (see Table 3 for the PLQY values) are shown in black. Although there are large deviations among the PLQY values for a given Cu···O distance, there is a general trend for increased PLQY values with longer Cu···O separations. The larger spread of Cu···O distances for [Cu(POP)(N^N][X] compounds reflects the greater flexibility of the POP ligand with respect to xantphos. With a couple of exceptions ([Cu(xantphos)(**2**)][PF_6] being one of them), photoluminescence is generally weak when Cu···O < 3.10 Å. In general, the longest Cu···O distances and highest PLQY values appear in [Cu(xantphos)(N^N]$^+$ cations. Interestingly, however, the highest PLQYs are for complexes containing the POP ligand in which N^N = 4,4′-bis(4-fluorophenyl)-6,6′-dimethyl-2,2′-bipyridine (CSD refcode EVAFAK and PLQY = 74% [31]), 4,4′,6,6′-tetramethyl-2,2′-bipyridine (CSD refcode COYHEF and PLQY = 55% [38]), and 6,6′-dimethyl-2,2′-bipyridine (CSD refcode BOSYUF and PLQY = 43.2% [8]).

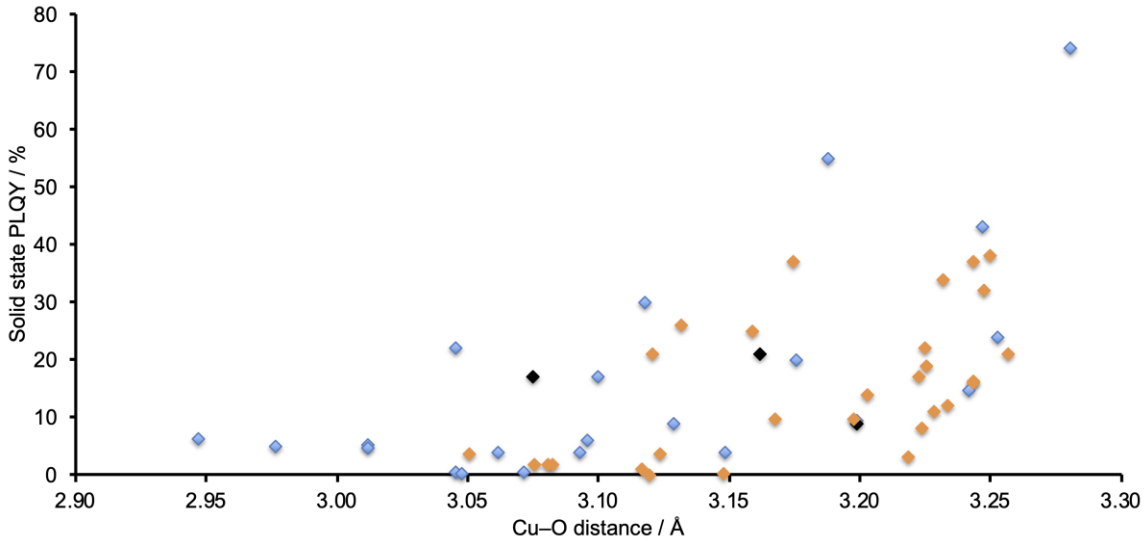

Figure 12. Solid-state PLQY values as a function of crystallographically determined Cu···O distances for [Cu(POP)(N^N)]$^+$ (blue markers) and [Cu(xantphos)(N^N)]$^+$ (orange markers) in which N^N is bpy or a functionalized bpy, compared with data for [Cu(POP)(**2**)][PF_6], [Cu(xantphos)(**1**)][PF_6], and [Cu(xantphos)(**2**)][PF_6] (black markers).

4. Conclusions

We prepared and characterized the compounds [Cu(POP)(**1**)][PF_6], [Cu(POP)(**2**)][PF_6], [Cu(xantphos)(**1**)][PF_6], and [Cu(xantphos)(**2**)][PF_6] in which ligands **1** and **2** contain an extended π-system with respect to the commonly employed bpy domain. Single crystal structures of [Cu(POP)(**2**)][PF_6], [Cu(xantphos)(**1**)][PF_6], and [Cu(xantphos)(**2**)][PF_6] were determined and confirmed a distorted copper(I) coordination environment in each complex. In the xantphos-containing complexes, ligand **1** is positioned with the quinoline over the xanthene unit, while ligand

2 is oriented with the 6-methylpyridine group facing the xanthene unit. ^{1}H NMR spectroscopic data are consistent with this difference persisting in solution. The [Cu(POP)(**2**)]$^+$, [Cu(xantphos)(**1**)]$^+$, and [Cu(xantphos)(**2**)]$^+$ cations present different edge-to-face and face-to-face π-interactions. In [Cu(POP)(**2**)][PF_6], pairs of cations associate through an efficient π-stacking embrace. This possibly contributes to a PLQY value of 21% for powdered [Cu(POP)(**2**)][PF_6], this being the highest PLQY of the four compounds. The design of new ligands to enhance the PL properties of [Cu(P^P)(N^N)]$^+$ complexes is critical for the advancement of LEC technology, and we have offered some thoughts on the role of π-stacking interactions and on Cu···O distances in the {Cu(POP)} and {Cu(xantphos)} domains.

Supplementary Materials: The following are available online at www.mdpi.com/2073-4352/10/4/255/s1, Figures S1–S4: mass spectra of the copper(I) compounds; Figures S5–S12: HMQC and HMBC spectra of the copper(I) compounds; Figures S13–24: Solid-state lifetime decay and first-order fitting curves, and IRF; Table S1: summary of data from the CSD used for Figure 12.

Author Contributions: Conceptualization, supervision, project administration, funding acquisition (C.E.H.; E.C.C.); investigation, data analysis (S.K.; M.A-Z.); crystallography (A.P.); manuscript writing (C.E.H.); manuscript editing (all authors). All authors have read and agreed to the published version of the manuscript.

Funding: This research was funded in part by the Swiss National Science Foundation, grant number 200020_162631.

Acknowledgments: We thank the University of Basel for support of our research. We acknowledge the assistance of Marco Meyer, Nina Arnosti and Fabian Brunner (all from the University of Basel) in recording the absorption spectra, some of the electrospray mass spectra and for assistance in collating final analytical data.

Conflicts of Interest: The authors declare no conflict of interest.

References

1. Kamer, P.C.J.; van Leeuwen, P.W.N.M.; Reek, J.N.H. Wide Bite Angle Diphosphines: Xantphos Ligands in Transition Metal Complexes and Catalysis. *Acc. Chem. Rev.* **2001**, *34*, 895–904, doi:10.1021/ar000060.
2. Costa, R.D. *Light-Emitting Electrochemical Cells: Concepts, Advances and Challenges*; Springer International Publishing: New York, NY, USA, 2017, doi:10.1007/978-3-319-58613-7.
3. Fresta, E.; Costa, R.D. Beyond traditional light-emitting electrochemical cells – a review of new device designs and emitters. *J. Mater. Chem. C* **2017**, *5*, 5643–5675, doi:10.1039/C7TC00202E.
4. Buckner, M.T.; McMillin, D.R. Photoluminescence from copper(I) complexes with low-lying metal-to-ligand charge transfer excited states. *J. Chem. Soc. Chem. Commun.* **1978**, 759–761, doi:10.1039/C39780000759.
5. Rader, R.A.; McMillin, D.R.; Buckner, M.T.; Matthews, T.G.; Casadonte, D.J.; Lengel, R.K.; Whittaker, S.B.; Darmon, L.M.; Lytle, F.E. Photostudies of 2,2′-bipyridine bis(triphenylphosphine)copper(1+), 1,10-phenanthroline bis(triphenylphosphine)copper(1+), and 2,9-dimethyl-1,10-phenanthroline bis(triphenylphosphine)copper(1+) in solution and in rigid, low-temperature glasses. Simultaneous multiple emissions from intraligand and charge-transfer states. *J. Am. Chem. Soc.* **1981**, *103*, 5906–5912, doi:10.1021/ja00409a048.
6. Czerwieniec, R.; Leitl, M.J.; Homeier, H.H.H.; Yerson, H. Cu(I) complexes—Thermally activated delayed fluorescence. Photophysical approach and material design. *Coord. Chem. Rev*. **2016**, *325*, 2–28, doi:10.1016/j.ccr.2016.06.016.
7. Bergmann, L.; Zink, D.M.; Bauman, T.; Volz, D.; Bräse, S. Metal-Organic and Organic TADF Materials: Status, Challenges and Characterization. *Top. Curr. Chem*. **2016**, *374*, 22.doi:10.1007/s41061-016-0022-6.
8. Keller, S.; Constable, E.C.; Housecroft, C.E.; Neuburger, M.; Prescimone, A.; Longo, G.; Pertegás, A.; Sessolo, M.; Bolink, H.J. [Cu(bpy)(P^P)]$^+$ containing light-emitting electrochemical cells: Improving performance through simple substitution. *Dalton Trans.* **2014**, *43*, 16593–16596, doi:10.1039/c4dt02847c.
9. Keller, S.; Pertegás, A.; Longo, G.; Martínez, L.; Cerdá, J.; Junquera-Hernández, J.M.; Prescimone, A.; Constable, E.C.; Housecroft, C.E.; Ortí, E.; et al. Shine bright or live long: Substituent effects in [Cu(N^N)(P^P)]$^+$-based light-emitting electrochemical cells where N^N is a 6-substituted 2,2′-bipyridine. *J. Mater. Chem. C* **2016**, *4*, 3857–3871, doi:10.1039/C5TC03725E.
10. Alkan-Zambada, M.; Keller, S.; Martínez-Sarti, L.; Prescimone, A.; Junquera-Hernández, J.M.; Constable, E.C.; Bolink, H.J.; Sessolo, M.; Ortí, E.; Housecroft, C.E. [Cu(P^P)(N^N)][PF_6] compounds with

bis(phosphane) and 6-alkoxy, 6-alkylthio, 6-phenyloxy and 6-phenylthio-substituted 2,2′-bipyridine ligands for light-emitting electrochemical cells. *J. Mater. Chem. C* **2018**, *6*, 8460–8471, doi:10.1039/C8TC02882F.

11. Fresta, E.; Volpi, G.; Milanesio, M.; Garino, C.; Barolo, C.; Costa, R.D. Novel Ligand and Device Designs for Stable Light-Emitting Electrochemical Cells Based on Heteroleptic Copper(I) Complexes. *Inorg. Chem.* **2018**, *57*, 10469–10479, doi:10.1021/acs.inorgchem.8b01914.
12. Leoni, E.; Mohanraj, J.; Holler, M.; Mohankumar, M.; Nierengarten, I.; Monti, F.; Sournia-Saquet, A.; Delavaux-Nicot, B.; Nierengarten, J.-F.; Armaroli, N. Heteroleptic Copper(I) Complexes Prepared from Phenanthroline and Bis-Phosphine Ligands: Rationalization of the Photophysical and Electrochemical Properties. *Inorg. Chem.* **2018**, *57*, 15537–15549, doi:10.1021/acs.inorgchem.8b02879.
13. Carbonell-Vilar, J.M.; Fresta, E.; Armentano, D.; Costa, R.D.; Viciano-Chumillas, M.; Cano, J. Photoluminescent Cu(I) vs. Ag(I) complexes: Slowing down emission in Cu(I) complexes by pentacoordinate low-lying excited states. *Dalton Trans.* **2019**, *48*, 9765–9775, doi:10.1039/c9dt00772e.
14. Viciano-Chumillas, M.; Carbonell-Vilar, J.M.; Armentano, D.; Cano, J. Influence of Xantphos Derivative Ligands on the Coordination in Their Copper(I) and Silver(I) Complexes. *Eur. J. Inorg. Chem.* **2019**, 2982–2989, doi:10.1002/ejic.201900323.
15. Costa, R.D.; Tordera, D.; Ortí, E.; Bolink, H.J.; Schönle, J.; Graber, S.; Housecroft, C.E.; Constable, E.C.; Zampese, J.A. Copper(I) Complexes for Sustainable Light-Emitting Electrochemical Cells. *J. Mater. Chem.* **2011**, *21*, 16108–16118, doi:10.1039/c1jm12607e.
16. Keller, S.; Brunner, F.; Junquera-Hernández, J.M.; Pertegás, A.; La-Placa, M.-G.; Prescimone, A.; Constable, E.C.; Bolink, H.J.; Ortí, E.; Housecroft, C.E. CF_3 Substitution of [Cu(P^P)(bpy)][PF_6] complexes: Effects on Photophysical Properties and Light-emitting Electrochemical Cell Performance. *ChemPlusChem* **2018**, *83*, 217–229, doi:10.1002/cplu.201700501.
17. Yang, L.; Feng, J.-K.; Ren, A.-M.; Zhang, M.; Ma, Y.-G.; Liu, X.-D. Structures, Electronic States and Electroluminescent Properties of a Series of Cu^{I} Complexes. *Eur. J. Inorg. Chem.* **2005**, *2005*, 1867–1879, doi:10.1002/ejic.200400941.
18. Kubas, G.J.; Monzyk, B.; Crumbliss, A.L. Tetrakis(acetonitrile)copper(I) hexafluorophosphate. *Inorg. Synth.* **1979**, *19*, 90–92, doi:10.1002/9780470132500.ch18.
19. Uenishi, J.; Tanaka, T.; Nishiwaki, K.; Wakabayashi, S.; Oae, S.; Tsukube, H. Synthesis of ω-(Bromomethyl)bipyridines and Related to ω-(Bromomethyl)pyridinoheteroaromatics: Useful Functional Tool for Ligands in Host Molecules. *J. Org. Chem.* **1993**, *58*, 4382–4388, doi:10.1021/jo00068a037.
20. Liu, Y.; Chen, F.; He, Y.-M.; Li, C.; Fan, Q.-H. Enantioselective Synthesis of Tunable Chiral Pyridine–Aminophosphine Ligands and Their Application in Asymmetric Hydrogenation. *Org. Biomol. Chem*. **2019**, *17*, 5099–5105, doi:10.1039/C9OB00770A.
21. Software for the Integration of CCD Detector System Bruker Analytical X-ray Systems; Bruker Axs: Madison, WI, USA, 2013.
22. Betteridge, P.W.; Carruthers, J.R.; Cooper, R.I.; Prout, K.; Watkin, D.J. CRYSTALS version 12: Software for guided crystal structure analysis. *J. Appl. Cryst*. **2003**, *36*, 1487–1487, doi:10.1107/S0021889803021800.
23. Palatinus, L.; Chapuis, G. Superflip-A Computer Program for the Solution of Crystal Structures by Charge Flipping in Arbitrary Dimensions. *J. Appl. Cryst.* **2007**, *40*, 786–790, doi:org/10.1107/S0021889807029238.
24. Palatinus, L.; Prathapa, S.J.; van Smaalen, S. EDMA: A Computer Program for Topological Analysis of Discrete Electron Densities. *J. Appl. Cryst.* **2012**, *45*, 575–580, doi:org/10.1107/S0021889812016068.
25. Dolomanov, O.V.; Bourhis, L.J.; Gildea, R.J.; Howard, J.A.K.; Puschmann, H. Olex2: A Complete Structure Solution, Refinement and Analysis Program. *J. Appl. Cryst.* **2009**, *42*, 339–341, doi:org/10.1107/S0021889808042726.
26. Macrae, C.F.; Edgington, P.R.; McCabe, P.; Pidcock, E.; Shields, G.P.; Taylor, R.; Towler, M.; van de Streek, J. Mercury: Visualization and analysis of crystal structures. *J. Appl. Cryst.* **2006**, *39*, 453–457, doi:10.1107/S002188980600731X.
27. Macrae, C.F.; Bruno, I.J.; Chisholm, J.A.; Edgington, P.R.; McCabe, P.; Pidcock, E.; Rodriguez-Monge, L.; Taylor, R.; van de Streek, J.; Wood, P.A. Mercury CSD 2.0-new features for the visualization and investigation of crystal structures. *J. Appl. Cryst*. **2008**, *41*, 466–470, doi:org/10.1107/S0021889807067908.
28. Spartan ‘18 version 1.3; Wavefunction INC.: Irvine, CA 92612, USA.

29. Yang, L.; Powell, D.R.; Houser, R.P. Structural variation in copper(I) complexes with pyridylmethylamide ligands: Structural analysis with a new four-coordinate geometry index, τ_4. *Dalton Trans*. **2007**, 955–964, doi:10.1039/b617136b.
30. Groom, C.R.; Bruno, I.J.; Lightfoot, M.P.; Ward, S.C. The Cambridge Structural Database. *Acta Cryst.* **2016**, *72*, 171–179, doi:10.1107/S2052520616003954.
31. Brunner, F.; Martínez-Sarti, L.; Keller, S.; Pertegás, A.; Prescimone, A.; Constable, E.C.; Bolink, H.J.; Housecroft, C.E. Peripheral halo-functionalization in $[Cu(N^N)(P^P)]^+$ emitters: Influence on the performances of light-emitting electrochemical cells. *Dalton Trans.* **2016**, *45*, 15180–15192, doi:10.1039/c6dt02665f.
32. McCullough, B.J.; Neyhouse, B.J.; Schrage, B.R.; Reed, D.T.; Osinski, A.J.; Ziegler, C.J.; White, T.A. Visible-Light-Driven Photosystems Using Heteroleptic Cu(I) Photosensitizers and Rh(III) Catalysts To Produce H_2. *Inorg. Chem.* **2018**, *57*, 2865–2875, doi:10.1021/acs.inorgchem.7b03273.
33. Kubiček, K.; Veedu, S.T.; Storozhuk, D.; Kia, R.; Techert, S. Geometric and electronic properties in a series of phosphorescent heteroleptic Cu(I) complexes: Crystallographic and computational studies. *Polyhedron* **2017**, *124*, 166–176, doi:10.1016/j.poly.2016.12.035.
34. Zhang, Q.; Ding, J.; Cheng ,Y.; Wang, L.; Xie, Z.; Jing, X.; Wang, F. Novel Heteroleptic Cu^I Complexes with Tunable Emission Color for Efficient Phosphorescent Light-Emitting Diodes. *Adv. Funct. Mater.* **2007**, *17*, 2983–2990, doi:10.1002/adfm.200601053.
35. Bruno, I.J.; Cole, J.C.; Edgington, P.R.; Kessler, M.; Macrae, C.F.; McCabe, P.; Pearson, J.; Taylor, R. New software for searching the Cambridge Structural Database and visualising crystal structures. *Acta Cryst*. **2002**, *58*, 389–397, doi:10.1107/S0108768102003324.
36. Janiak, C. A critical account on π–π stacking in metal complexes with aromatic nitrogen-containing ligands. *J. Chem. Soc. Dalton Trans.* **2000**, 3885–3896, doi:10.1039/B003010O.
37. Kuang, S.-M.; Cuttell, D.G.; McMillin, D.R.; Fanwick, P.E.; Walton, R.A. Synthesis and Structural Characterization of Cu(I) and Ni(II) Complexes that Contain the Bis[2-(diphenylphosphino)phenyl]ether Ligand: Novel Emission Properties for the Cu(I) Species. *Inorg. Chem.* **2002**, *41*, 3313–3323, doi:10.1021/ic0201809.
38. Linfoot, C.L.; Leitl, M.J.; Richardson, P.; Rausch, A.F.; Chepelin, O.; White, F.J.; Yersin, H.; Robertson, N. Thermally Activated Delayed Fluorescence (TADF) and Enhancing Photoluminescence Quantum Yields of $[CuI(diimine)(diphosphine)]^+$ Complexes—Photophysical, Structural, and Computational Studies. *Inorg. Chem*. **2014**, *53*, 10854–10861, doi:10.1021/ic500889s.